Diagnostic studies of the dynamical behaviour of the ECMWF model

By **Mike Cullen**

European Centre for Medium-Range Weather Forecasts

Abstract

The dynamical behaviour of the ECMWF model is illustrated using two forms of analysis. The first is a decomposition of short range forecast differences into balanced and unbalanced parts, which illustrates the degree of balance in the model, the nature of the imbalances, and the correlation of differences in the moisture and ozone fields with the dynamical variables. The second is a study of the behaviour of different versions of the semi-implicit scheme. This is illustrated both with diagnostics of the time variability of the model, and with diagnostics that measure the low frequency gravity wave activity compared with the synoptic activity.

1. Introduction

This paper discusses two forms of diagnostic study which focus on the dynamical behaviour of the ECMWF model. Both areas of study are ongoing. The purpose of this paper is to describe results to date as an illustration of the use of various of diagnostic methods. Many of the issues identified require considerable further work and are likely to be the subject of future papers.

The first study examines the statistics of short range forecast errors generated by two different methods. The errors are projected onto 'balanced' and 'unbalanced' components using a standard linear change of variables. The balanced part essentially corresponds to potential vorticity, and the unbalanced part to the departure from linear balance. It is shown that these two components of the errors are essentially uncorrelated, which supports the relevance of this decomposition. The degree of balance appears to depend strongly on the length of the forecast used to generate the errors. The unbalanced component is found to project strongly onto the temperature field, this is shown to imply that the imbalance is mainly on horizontal scales smaller than the Rossby radius of deformation. The correlations between these components of the error and those of the divergent wind, moisture and ozone are then calculated. It is found that there is a large correlation between the unbalanced part of the vorticity and height errors and the moisture, divergence and ozone errors.

The second study is into the performance of the semi-implicit scheme used in the ECMWF model. The diagnostics calculated measure the degree of variability in the divergence on the timescale of the model timestep, and compare it with expectations based on asymptotic theory. Estimates are also made of the degree of low frequency inertio-gravity wave activity by studying statistics of the vertical motion and precipitation fields. It is found that there is substantial activity on the scale of the timestep, and that the physics increments generate a large fraction of this. However, improved techniques which reduce the high frequency forcing do not have a large impact on overall performance. Techniques designed to achieve more accurate treatment of the asymptotic solution in the presence of high frequency gravity waves are shown to have a beneficial impact on overall performance, but little impact on apparently incorrect low frequency vertical motions. Filtering which damps motions with rapid variations along trajectories does reduce the latter motions, though there is some effect on synoptic fields as well.

2. DIAGNOSTICS OF SHORT RANGE FORECAST ERRORS

2.1 Method of analysis

We write the linearised discrete equations of the ECMWF model for a single total wavenumber n as, (*Simmons and Temperton*, 1997):

$$
\begin{aligned}
D^+ - D^0 &= \mathcal{D} + \frac{n(n+1)}{a^2}(\gamma\bar{T} + \sigma\bar{p}_{surf}) + \omega\bar{\varsigma} \qquad (1)\\
\varsigma^+ - \varsigma^0 &= \mathcal{Z} - \omega\bar{D}\\
T^+ - T^0 &= \mathcal{T} - \tau\bar{D}\\
p^+_{surf} - p^0_{surf} &= \mathcal{P} - \nu\bar{D}
\end{aligned}
$$

where $D, \varsigma, T, p_{surf}$ represent divergence, vorticity, temperature and surface pressure, overbars indicate averages over a timestep which takes initial values with superscript 0 to final values with superscript +. Script terms represent nonlinear terms and Greek letters matrix operators. Define a linearised potential vorticity by

$$Q = (\gamma\tau + \sigma\nu)\varsigma - \omega(\gamma T + \sigma p_{surf}) \qquad (2)$$

This obeys the equation

$$Q^+ - Q^0 = \mathcal{Q} - (\gamma\tau + \sigma\nu)\omega D + \omega(\gamma\tau + \sigma\nu)D \qquad (3)$$

The matrices ω, which only relate horizontal wavenumbers, and $\gamma\tau + \sigma\nu$, which only relate vertical levels, commute, and so Q is conserved by the linear part of the equations. It actually represents a vertical integral of the quasi-geostrophic potential vorticity. Define the 'linear imbalance' as

$$R = \frac{n(n+1)}{a^2}(\gamma T + \sigma p_{surf}) + \omega\varsigma \qquad (4)$$

(2) and (4) allow us to decompose a general set of vorticity, temperature and surface pressure differences $\varsigma', T', p_{surf}'$ into potential vorticity and linear imbalance differences. We can also invert these relationships to obtain

$$
\begin{aligned}
\left(\omega^2 + \frac{n(n+1)}{a^2}(\gamma\tau + \sigma\nu)\right)\phi' &= (\gamma\tau + \sigma\nu)R' - \omega Q' \qquad (5)\\
\left(\frac{\omega a^2\omega}{n(n+1)} + (\gamma\tau + \sigma\nu)\right)\varsigma' &= \frac{\omega a^2}{n(n+1)}R' + Q'
\end{aligned}
$$

where $\phi' = \gamma T' + \sigma p'_{surf}$. Care has to be taken because ω does not commute with $n(n+1)$. On the ECMWF vertical grid, the matrix operator defining ϕ has a kernel. This component of the T, p_{surf} differences has to be calculated and kept separately.

Apply this decomposition to a single total wavenumber n and assume a constant Coriolis parameter f. Consider a single eigenmode of the $\gamma\tau + \sigma\nu$ matrix, with eigenvalue ϕ_0. Then (2) and (4) become

$$Q' = \phi_0 \varsigma' - f\phi' \tag{6}$$
$$R' = \frac{n(n+1)}{a^2}\phi' + f\varsigma'$$

and (5) becomes

$$\left(f^2 + \frac{n(n+1)}{a^2}\phi_0\right)\phi' = \phi_0 R' - fQ' \tag{7}$$
$$\left(\frac{f^2a^2}{n(n+1)} + \phi_0\right)\varsigma' = \frac{fR'a^2}{n(n+1)} + Q'$$

Given a difference ϕ' with $\varsigma' = 0$, we can thus write

$$\left(f^2 + \frac{n(n+1)}{a^2}\phi_0\right)\phi'_R = \frac{n(n+1)}{a^2}\phi_0\phi' \tag{8}$$
$$\left(f^2 + \frac{n(n+1)}{a^2}\phi_0\right)\phi'_Q = f^2\phi'$$
$$\phi' = \phi'_R + \phi'_Q$$

Thus if the horizontal scale is larger than the Rossby radius of deformation for the given vertical structure, which means

$$a^2f^2 > \phi_0 n(n+1) \tag{9}$$

then $\phi'_Q > \phi'_R$ and height differences largely project onto the potential vorticity. Similar algebra gives

$$\left(\frac{f^2a^2}{n(n+1)} + \phi_0\right)\varsigma'_R = \frac{f^2a^2}{n(n+1)}\varsigma' \tag{10}$$
$$\left(\frac{f^2a^2}{n(n+1)} + \phi_0\right)\varsigma'_Q = \phi_0\varsigma'$$

(10) shows that, on scales larger than the Rossby radius of deformation, vorticity differences largely project onto the linear imbalance.

We decompose given sets of short range forecast differences into potential vorticity and linear imbalance, and illustrate what proportion of the height and vorticity errors are accounted for by the two components. We calculate the variance in the 'kernel' mode of T, p_{surf} differences which are invisible to the height error. We also calculate the correlations of short range forecast differences in horizontal divergence, moisture, and ozone with the differences in Q and R.

2.2 Results

The analysis was carried out using two sets of forecast differences. The first (experiment A) uses 138 differences between pairs of 6 hour forecasts derived from independent analyses of the same observations generated by M.Fisher. The technique of setting up an ensemble of analyses in this way is described by *Houtekamer and Mitchell* (1998). The data were derived from a 60 level version of the ECMWF model. The second (experiment B) uses the 'NMC' method , *Parrish and Derber* (1992), of comparing 24 and 48 hour forecasts valid at the same time, and was derived from operational T319L31 ECMWF forecasts. 50 pairs were used. The sample size needs to be greater than the number of levels for the correlations derived statistically to have any validity.

TABLE 1 . VARIANCES FOR EXPERIMENT A (% OF TOTAL)

Variable	Q part	R part	uncorrelated with either	total of components
Vorticity	88	13	0	101
Temperature	27	77	0.01	104
Surface pressure	53	36	0	89
Divergence	1.4	59	50	110
Moisture	2.2	30	69	101
Ozone	7	18	75	100

TABLE 2 . VARIANCES FOR EXPERIMENT B(% OF TOTAL)

Variable	Q part	R part	uncorrelated with either	total of components
Vorticity	96	4	0	100
Temperature	88	28	0	116
Surface pressure	75	9	0	84
Divergence		19	84	103
Moisture		3	98	101

The standard deviations of the decomposition of the vorticity, temperature, and surface pressure errors for different total wavenumber groups are shown in Fig.1 for experiment A. The variances have been accumulated over blocks of 5 wavenumbers, and the standard deviations calculated from them.

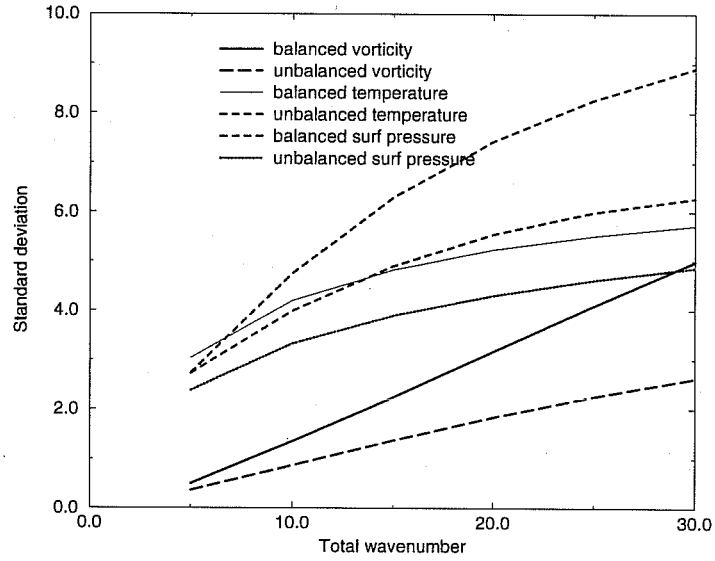

Figure 1:

The results from experiment A show a substantial amount of imbalance, which largely projects onto the temperature and surface pressure. Since the scale dependence of the decomposition in section 2.1 is fixed, this means that the errors are largely on scales smaller than the Rossby radius, so that $a^2f^2 < \phi_0 n(n+1)$. In experiment B the proportion of variance projecting onto the unbalanced mode is much smaller. It is likely that the difference explained by the longer period of forecast used to estimate the errors. In experiment A the forecasts were only for 6 hours, in experiment B they were 24 and 48 hours. Other possible contributors are the increased vertical resolution in experiment A, and the use of random perturbations to the physical increments in the model used to generate the ensemble of analyses. Further experimentation is required to determine which is the main cause of the different results. Further experiments are also needed to establish why most of the imbalance is on scales smaller than the Rossby radius. This could reflect the nature of the analysis increments, the imbalance coming fron the use of the perturbations to the physical increments, or the ability of the model to adjust on different scales. However, theoretically, the adjustment process should be most effective on scales smaller than the Rossby radius where gravity waves are fast. The first two possibilities are thus the more likely.

There is very little variance in the 'kernel' mode, which is invisible to the pressure field. This suggests that the model formulation is sufficiently smooth in the vertical to avoid exciting this mode.

It is interesting to observe the strong correlations between divergence and imbalance and moisture and imbalance. The latter suggests that vertical motion errors explain a substantial part of moisture errors, which is to be expected given the strong vertical gradient of atmospheric moisture content. A larger correlation could be expected, if it were not for the fact that there is considerable moisture transport within the parametrization schems, and there may not be a strong correlation between vertical motion errors and errors in parametrized mass transport. There is a noticeable correlation between ozone errors and potential vorticity errors. This may result from a correlation between potential vorticity errors and tropopause height errors. In the case of moisture, this effect would be swamped by the larger moisture errors at low levels. Further study is required to explore these relationships.

3. DIAGNOSTICS FROM THE SEMI-IMPLICIT DYNAMICS

The use of efficient semi-implicit, semi-Lagrangian schemes in the ECMWF and many other models is motivated by the fact that only a small amount of the atmospheric variability which can be resolved by large scale models is described by motions which vary on faster than advective timescales. Mathematicians, e.g. *Browning and Kreiss* (1986), have demonstrated that in this situation the flow can be approximately described by a balanced system of equations, and have also made estimates of the difference between the exact solution and the balanced solution. In this study we carry out a diagnostic study of how close the model is to balance. This is a test of the validity of the aysmptotic analysis, and thus of the appropriateness of the choice of a semi-implicit, semi-Lagrangian integration scheme. It also tests the ability of the integration scheme to maintain the asymptotic regime.

3.1 Asymptotic analysis

We use the continuous equations from which (1) are derived as our basic equation set, but work directly with the vertically discrete form:

$$\frac{\partial D}{\partial t} = \mathcal{D} - \nabla^2(\gamma T + \sigma p_{surf}) + \omega\varsigma \tag{11}$$

$$\frac{\partial \varsigma}{\partial t} = \mathcal{Z} - \omega D$$

$$\frac{\partial T}{\partial t} = \mathcal{T} - \tau D$$

$$\frac{\partial p_{surf}}{\partial t} = \mathcal{P} - \nu D$$

These imply an equation for the second time derivative of the divergence of the form

$$\frac{\partial^2 D}{\partial t^2} = \nabla^2(\gamma\tau + \sigma\nu)D - \omega^2 D + \mathcal{F} \tag{12}$$

$$= LD + \mathcal{F}$$

The operator L has eigenvalues corresponding to inertio-gravity waves. Assume that the inertio-gravity wave timescale is $O(\varepsilon)$, $\varepsilon \ll 1$, and that the forcing term $\mathcal{F}$ is on the 'slow' timescale of order 1. Thus $L = O(\varepsilon^{-2})$. Then, following *Ford et al.* (1999), for instance, we have

$$\frac{\partial^2}{\partial t}(D_b + D_u) = L(D_b + D_u) + \mathcal{F} \tag{13}$$

where we define

$$LD_b + \mathcal{F} = 0 \tag{14}$$

and so

$$\frac{\partial^2 D_u}{\partial t^2} = LD_u - \frac{\partial^2 D_b}{\partial t^2} \tag{15}$$

Both terms in (14) are O(1), so D_b is $O(\varepsilon^2)$. All terms in (15) are then $O(\varepsilon^2)$, because D_b only varies on the slow O(1) timescale, so $D_u = O(\varepsilon^4)$.

In the forecast model, assume that $D_u = \alpha D_b$. We can estimate α by calculating the ratio of the r.m.s. values of $\delta_{tt}D \equiv D_{t+\Delta t} - 2D_t + D_{t-\Delta t}$ and D. Assume the timestep is μ, where the use of a semi-implicit scheme means that $\mu \gg \varepsilon$, but the need for accuracy means that $\mu \ll 1$, the slow timescale. Then we have

$$\frac{\|\delta_{tt}D\|}{\|D\|} = \frac{\mu^2 + \alpha}{1 + \alpha} \sim \alpha \tag{16}$$

and similarly

$$\frac{\|\delta_{tt}D\|}{\|\delta_t D\|} = \frac{\mu^2 + \alpha}{\mu + \alpha} \tag{17}$$

The semi-implicit scheme ensures that $\mu \gg \varepsilon$, and we hope that $\alpha = O(\varepsilon^2)$. Then $\mu \gg \alpha$, so that the ratio in (17) is $O(\mu)$. If $\alpha = O(\mu)$, on the other hand, the ratio will be O(1), and the asymptotic solution will not be being followed. Note that if there is only a single time scale present, the value of (16) will be the square of the value of (17).

Another, related, diagnostic is the ratio of the semi-implicit correction to the initial estimate of the divergence tendency. The semi-implicit approximation to (11) can be written as

$$\begin{aligned} D_{t+\Delta t} &= D_t + \Delta t(\mathcal{D} - \nabla^2(\gamma_r T + \sigma_r p_{surf}) + \omega_r \varsigma)_t \\ &+ \frac{1}{4}\Delta t^2(\nabla^2(\gamma_r \tau_r + \sigma_r \nu_r)D_{t+\Delta t} + \omega_r D_{t+\Delta t} + \mathcal{G}) \\ &= D_t + \Delta t D_1 + \frac{1}{4}\Delta t^2 D_2 \end{aligned} \tag{18}$$

The suffix r on the matrices indicates that they are derived from a reference state. We calculate the ratio $\frac{1}{4}\Delta t(\|D_2\|/\|D_1\|)$. This should be equal to the ratio $\frac{1}{4}(\|\delta_{tt}D\|/\|\delta_t D\|)$ for the centred time differencing used in (18), and $\|\delta_{tt}D\|/\|\delta_t D\|$ for backward time differencing, but in practice will be affected by the linearisation carried out within the semi-implicit step.

3.2 Experiments

Five different versions of the ECMWF model were evaluated using these diagnostics. In each case, 12 forecasts were run from the 15th of every month in 1998 starting with the operational analysis. The resolution used was T319L31, which was the operational resolution for most of 1998. The r.m.s values of the diagnosed fields were

calculated for each case, and then averaged over the 12 cases. Brief descriptions of each model version are given below.

Experiment 1 is a set of control forecasts using the standard version of the semi-implicit scheme, *Temperton* (1997). This is equivalent to first solving (18) to estimate $D_{t+\Delta t} - D_t \equiv D'$, followed by setting

$$\begin{aligned} \varsigma_{t+\Delta t} &= \varsigma_t + \Delta t\left(\mathcal{Z} - \omega D_t - \frac{1}{2}\omega_r D'\right) \\ T_{t+\Delta t} &= T_t + \Delta t\left(\mathcal{T} - \tau D_t - \frac{1}{2}\tau_r D'\right) \\ (p_{surf})_{t+\Delta t} &= (p_{surf})_t + \Delta t\left(\mathcal{P} - \nu D_t - \frac{1}{2}\nu_r D'\right) \end{aligned} \tag{19}$$

Experiment 2 solves (18) to estimate $D_{t+\Delta t}$, followed by setting

$$\begin{aligned} \varsigma_{t+\Delta t} &= \varsigma_t + \Delta t(\mathcal{Z} - \omega \overline{D}^t) \\ T_{t+\Delta t} &= T_t + \Delta t(\mathcal{T} - \tau \overline{D}^t) \\ (p_{surf})_{t+\Delta t} &= (p_{surf})_t + \Delta t(\mathcal{P} - \nu \overline{D}^t) \end{aligned} \tag{20}$$

Note the basic state matrices are no longer used in updating the vorticity and height fields, so can have no effect on the potential vorticity. A second iteration is carried out, setting

$$\begin{aligned} D_{t+\Delta t} &= D_t + \Delta t(\mathcal{D}_t - \nabla^2(\gamma_r \overline{T}^t + \sigma_r \overline{p}^t{}_{surf}) + \omega_r \overline{\varsigma}^t) \\ &+ \frac{1}{4}\Delta t^2(\nabla^2(\gamma_r \tau_r + \sigma_r \nu_r)D' + \omega_r D') \end{aligned} \tag{21}$$

and then solving (20) with D^t recalculated using (21). The overall impact of this experiment on forecast scores is small, as shown in Figure 2:

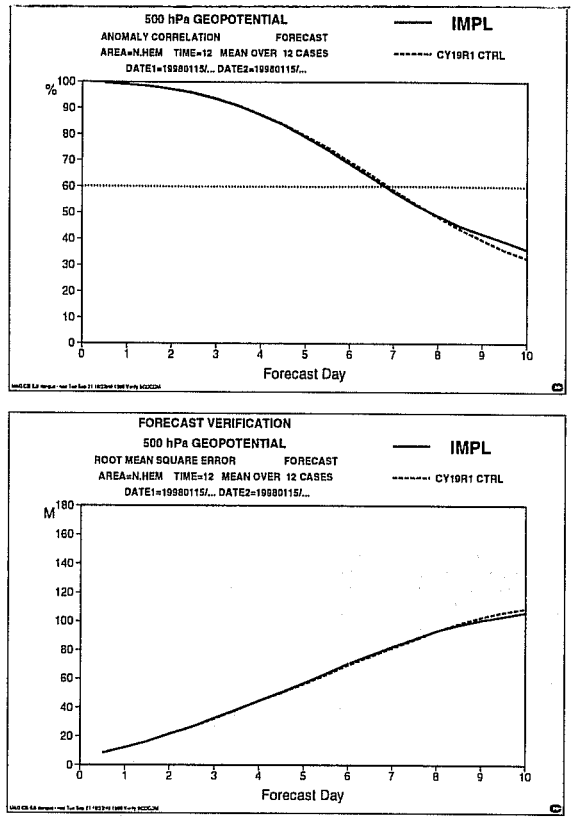

Figure 2: Scores from experiment 2

Experiment 3 tests a scheme developed by *Mohebalhojeh and Dritschel* (1999). This is designed to give the correct asymptotic limit of the solution of the shallow water equations as the gravity waves become faster. They showed that using this scheme allowed realistic predictions of the level of gravity wave activity under conditions where the flow was close to balance, though predictions of the evolution of individual gravity waves also required the use of a short timestep so that the Courant number for the waves was less than unity. The first step of the scheme can be written

$$\left(\frac{\partial D}{\partial t}\right)_t = \mathcal{D} - \nabla^2(\gamma T + \sigma p_{surf}) + \omega\varsigma \tag{22}$$

$$\left(\frac{\partial D}{\partial t}\right)_{t+\Delta t} = \left(\frac{\partial D}{\partial t}\right)_t + (\mathcal{D}_{t+\Delta t} - \mathcal{D}_t) - \Delta t\nabla^2(\gamma(\mathcal{T} - \tau D) + \sigma(\mathcal{P} - \nu D))$$

$$+ \omega\Delta t(\mathcal{Z} - \omega D)$$

$$D_{t+\Delta t} = D_t + \overline{\left(\frac{\partial D}{\partial t}\right)}^{t}$$

Given $\left(\frac{\partial D}{\partial t}\right)_{t+\Delta t}$, calculate D' such that

$$\mathcal{D}_{t+\Delta t} - \nabla^2(\gamma(T - \tau D') + \sigma(p_{surf} - \upsilon D')) + \omega(\varsigma - \omega D') = \left(\frac{\partial D}{\partial t}\right)_{t+\Delta t} \tag{23}$$

If the right hand side of (22) is time averaged, it is just a fully implicit treatment of the standard divergence equation. We solve it using an iteration equivalent to that used in experiment 2, using basic state matrices to make a first guess of $\left(\frac{\partial D}{\partial t}\right)_{t+\Delta t}$.

The key extra element which enforces the asymptotic solution is (23), because the D' that appears there does not change the divergence held as the history carrying variable. The scheme is has been found to be unstable in shallow water equation tests for small equivalent depths, so (23) is applied only to the first 10 vertical modes, and (22) alone is used for the higher modes. The results are shown in Fig.3.

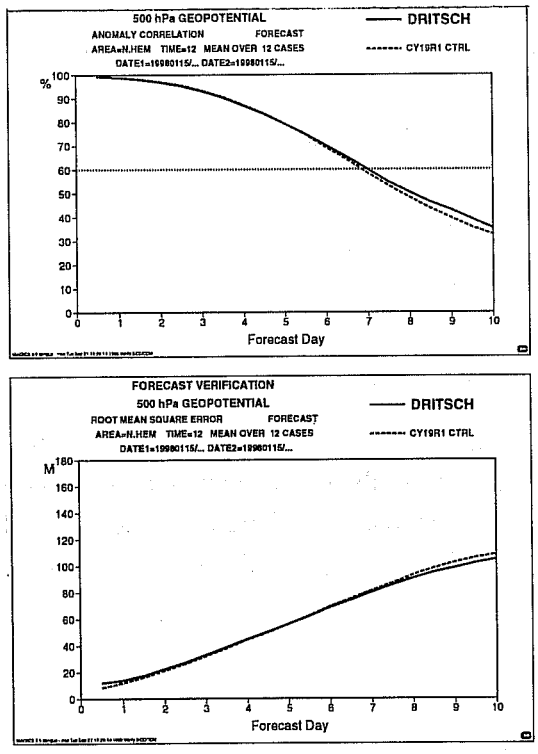

Figure 3: Results from experiment 3

Experiment 4 is the same as experiment 2, except that the centred time differencing used in the implicit calculations is replaced by backward time differencing, so that the linearised terms are evaluated only at time $t + \Delta t$. Since, in the semi-Lagrangian scheme, the values at time t were evaluated at departure points, this also removes the spatial averaging along trajectories. The impact on overall scores was quite large, as shown in Fig.4. Further experiments (not shown) indicated that the impact was derived from removing the spatial averaging rather than by altering the weighting of different time levels at the same point.

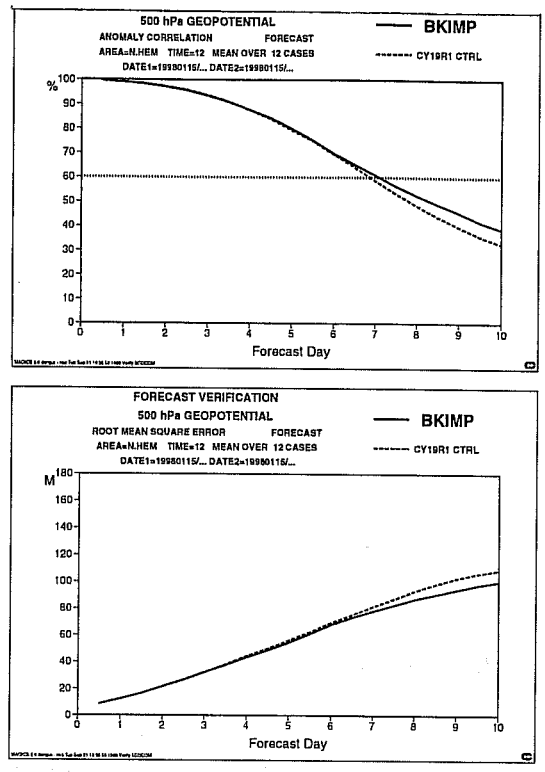

Figure 4: Results from experiment 4

The final experiment was to use the improved interfacing of the physics developed by *Wedi* (1999), in which the physics increments are treated as far as possible by averaging along the trajectory, as with the dynamics increments, and using a common set of input fields for all the physical processes. The operational scheme up to July 1999 used the output from each process as input to the next. The effect on the overall model performance was small but positive. Many detailed aspects of performance were also improved.

3.3 Diagnostics from the semi-implicit scheme

Results from the diagnostic calculations described in 3.1 are shown in Table 3 .to Table 5 . The results are averaged over the 12 cases and are for 72 hour forecasts. The r.m.s values are calculated at levels 12 and 23 (approximately 275 and 710 hpa), and averaged over the two. They are shown separately for the northern hemisphere extratropics (20-90N), tropics (20S-20N) and southern hemisphere extratropics (20-90S).

TABLE 3 . NORTHERN EXTRATROPICS

	Expected value	Expt 1	2	3	4	5
$\delta_{tt}D/D$	α	0.214	0.203	0.206	0.186	0.129
$\delta_{tt}D/\delta_tD$	μ, 1	1.167	1.053	1.272	1.104	0.855
$\Delta tD_2/4D_1$	$(\mu, 1)/4$	0.253	0.806	0.995	1.645	0.247

TABLE 4 . TROPICS

	Expected value	Expt 1	Expt 2	Expt 3	Expt 4	Expt 5
$\delta_{tt}D/D$	α	0.166	0.178	0.281	0.145	0.092
$\delta_{tt}D/\delta_tD$	μ, 1	1.055	1.011	1.515	1.062	0.711
$\Delta tD_2/4D_1$	$(\mu, 1)/4$	0.499	1.309	0.675	2.388	0.336

TABLE 5 . SOUTHERN EXTRATROPICS

	Expected value	Expt 1	Expt 2	Expt 3	Expt 4	Expt 5
$\delta_{tt}D/D$	α	0.188	0.189	0.180	0.189	0.127
$\delta_{tt}D/\delta_tD$	μ, 1	0.994	0.887	1.123	1.009	0.755
$\Delta tD_2/4D_1$	$(\mu, 1)/4$	0.241	0.485	0.748	1.310	0.219

Some of the main features that these tables show are:

i) The values of $\delta_{tt}D/D$ are quite different from the squares of the values of $\delta_{tt}D/\delta_tD$. This is consistent with the presence of two timescales in the solution.

ii) All experiments have O(1) values of $\delta_{tt}D/\delta_tD$. This shows that the fast timescale is of order the timestep, and is consistent with (17) if $\alpha \sim O(\mu)$.

iii) All experiments except 5 have similar levels of fast wave activity, around 20%. Experiment 5 has around 13%. This suggest that physics increments are a major source of variability on the timescale of the model timestep, which can be improved on by better interfacing. However, there is only a small impact on overall model performance.

iv) The Courant number for the fastest waves is much greater than 1, so $\mu \gg \varepsilon$. Either the amplitude of these waves is much larger than the asymptotic value of $O(\varepsilon^2)$, or they are swamped by other waves for which the Courant number is O(1).

v) Additional experiments (not shown) with a timestep of 1800s showed a 4 times increase in the ratio $\delta_{tt}D/D$, more than the expected increase of 2.25.

vi) Experiment 3 has the largest values of $\delta_{tt}D/\delta_tD$, and in the tropics, of $\delta_{tt}D/D$ also. Since this scheme attempts to treat the level of fast wave activity accurately, the result suggests that there is considerable forcing on the timescale of the timestep. Experiment 5 suggests that a lot of this comes from the physics. Future work will combine experiments 3 and 5.

vii) Experiments 1 and 2 differ only in the formulation of the semi-implicit solution. The overall performance and the level of fast wave activity are similar in the two experiments. The difference in the semi-implicit solution procedure is seen in the value of (18). The expected value is observed in experiment 1, but in experiment 2 a larger divergence correction is needed to maintain stability. This is because the divergence correction is applied to the actual fields in (20), rather than basic state values as in (19). The larger divergence corrections are needed to give sufficient vorticity and height corrections. The split formulation in experiment 1 uses the same formulation in solving for $D_{t+\Delta t}$ as in updating the other fields, so the consistency with the

expected value of (18) is reasonable. Experiment 5 shares the formulation of experiment 1 and gives the same behaviour. In the decentered experiment, 4, the expected value of (18) is larger, but the actual value is larger still for the same reasons as in experiment 2.

The main lesson for model design from these diagnostics is the need to control the forcing on the timescale of the timestep, and to investiagte whether the dominant spatial scales associated with the timestep variability are associated with waves whose Courant number is much greater than 1 or of order 1. If the former, they should be damped since their amplitude would be unrealistically large. However, the link between variability on the scale of the timestep and large scale forecast scores appears rather weak.

3.4 Diagnostics of low frequency imbalance

Equation (12) implies the 'omega' equation (14), which shows that the level of balanced divergence is proportional to the time tendencies of the vorticity and height fields driven by the balanced motion, and to the physical forcing. A good diagnostic would be to compare the solution D_b, where the right hand side of (14) is derived from actual data, with the actual divergence. However, on small vertical scales we find that D_b then takes unrealistically large values. This is because the timestep is much shorter than the timescale associated with the operator L on these space scales. Applying L^{-1} to time tendencies derived from individual model timesteps is therefore a highly unstable procedure. The data would have to be averaged over an inertial period, which corresponds to the smallest eigenvalue of L (in the same way that physics tendencies have to be time averaged before use in diabatic normal mode initialisation). Thus, pending the development of such time-averaged diagnostic calculations, we assume that the r.m.s value of the right hand side of (14) is representative of a given level of synoptic variability, and can be estimated by the standard deviation of sea level pressure. (14) then implies that a particular level of balanced divergence will correspond to a given of synoptic variability. We can thus compare the degree of balance between different vesions of the model by comparing the ratio of r.m.s. divergence to the standard deviation of PMSL for the same cases. In addition, the precipitation fields provide a sensitive measure of the model's integrated vertical motion. It is therefore interesting to compare the standard deviations of precipitation rates (dynamic and convective) with the mean values, and see how the ratio depends on model formulation. In this case it is hard to say what is 'correct', but we should at least be able to understand the differences.

The experiments used are the same as those described in section 3.2. The r.m.s. vertical velocities are the average of the values at levels 12 and 23 at T+72, as for the diagnostics in section 3.3. The precipitation diagnostics are based on 12 hour accumulations from hours 60 to 72 of the forecasts. The definition of the areas is as in section 3.2.

TABLE 6 . NORTHERN EXTRATROPICS

Experiment	1	2	3	4	5
PMSL sd	990	989	974	960	989
W sd	4.14	4.14	4.12	3.63	4.02
ratio PMSL/W	239	239	236	264	246
LSP sd	102	102	101	101	98
mean	312	316	317	299	298
CP sd	28	29	30	30	27
mean	112	113	118	115	106

TABLE 7 . TROPICS

Experiment	1	2	3	4	5
PMSL sd	331	326	323	320	330
W sd	3.62	3.58	3.64	3.21	3.47
ratio PMSL/W	91	91	89	100	95
LSP sd	96	96	99	95	97
mean	262	265	288	268	282
CP sd	139	140	141	144	135
mean	263	267	291	277	258

TABLE 8 . SOUTHERN EXTRATROPICS

Experiment	1	2	3	4	5
PMSL sd	1689	1690	1676	1661	1688
W sd	4.10	4.00	3.98	3.50	3.90
ratio PMSL/W	412	423	421	475	433
LSP sd	118	118	117	116	113
mean	340	336	328	323	312
CP sd	21	21	21	22	20
mean	95	94	97	95	87

Some of the main points illustrated by these tables are:

i) The PMSL variance is almost the same in experiments 1,2 and 5. It is 1.5% less in the northern extratropics and 1% less in the southern extratropics in experiment 3 and 3% less in the northern extratropics and 2% less in the southern extratropics in experiment 4. In experiment 4, other diagnostics show that the global kinetic energy is reduced by 2.5% between days 0 and 5. This indicates that these versions of the model include some damping of the synoptic flow. It is impossible to determine whether this explains all the positive impact of both experiments on the large scale scores without further study.

ii) The ratio of the standard deviation of the vertical motion to that of the surface pressure is least for experiment 4 in all areas, showing that low frequency inertio-gravity waves are successfully damped more strongly than the synoptic flow. The ratio is also less in experiment 5, which is consistent with the reduced time variability in that experiment. It is similar in the other experiments, though in the tropics there is slightly more vertical motion in experiment 3, though not to the extent of the increased time variability shown in section 3.3.

iii) In the extratropics, experiment 5 produces least precipitation of both types, experiment 4 also produces less large scale precipitation (but not convection) than experiments 1-3. This suggests that better physics interfacing is beneficial in predicting precipitation rates. The standard deviation is also reduced, but not by as much as the mean. In experiment 4, the damping of vertical motion and surface pressure would be expected to give some reduction in large scale precipitation.

iv) In the tropics, experiments 4 and 5 produce more precipitation than experiments 1 and 2, and experiment 3 much more than either. In experiment 5 there is relatively more large scale precipitation, in the other experiemnts the ratio is similar. The standard deviations are less sensitive than the mean values. The change of precipitation type in experiment 5 probably reflects the diferent interfacing of processes. The increased precipitation in experiment 3 is consistent with the much higher time variability, and may reflect feedback between physical forcing on the scale of the timestep and more careful calculation of the response.

Overall the diagnostics suggest the importance of physics interfacing, especially if the integration scheme is made more accurate in treating fast responses, and illustrate that the decentering along trajectories in experiment 4 may be an effective way of reducing low frequency imbalance if that proves necessary.

3.5 Behavior near mountains

The previous subsections have concentrated on large scale average diagnostics. In this and the next two subsections we illustrate what they mean in terms of local behaviour

The first example is a case of flow over the Norwegian mountains, which appears typical of mid-latitude flow over orography. The satellite picture (Figure 5:) shows clear skies over the Baltic, cloud over the spine of the Norwegian mountains, and some bands of cloud parallel to the north-westerly wind downsream of the mountains. There may be some mountain wave activity, but this is uncertain from the resolution of the picture.

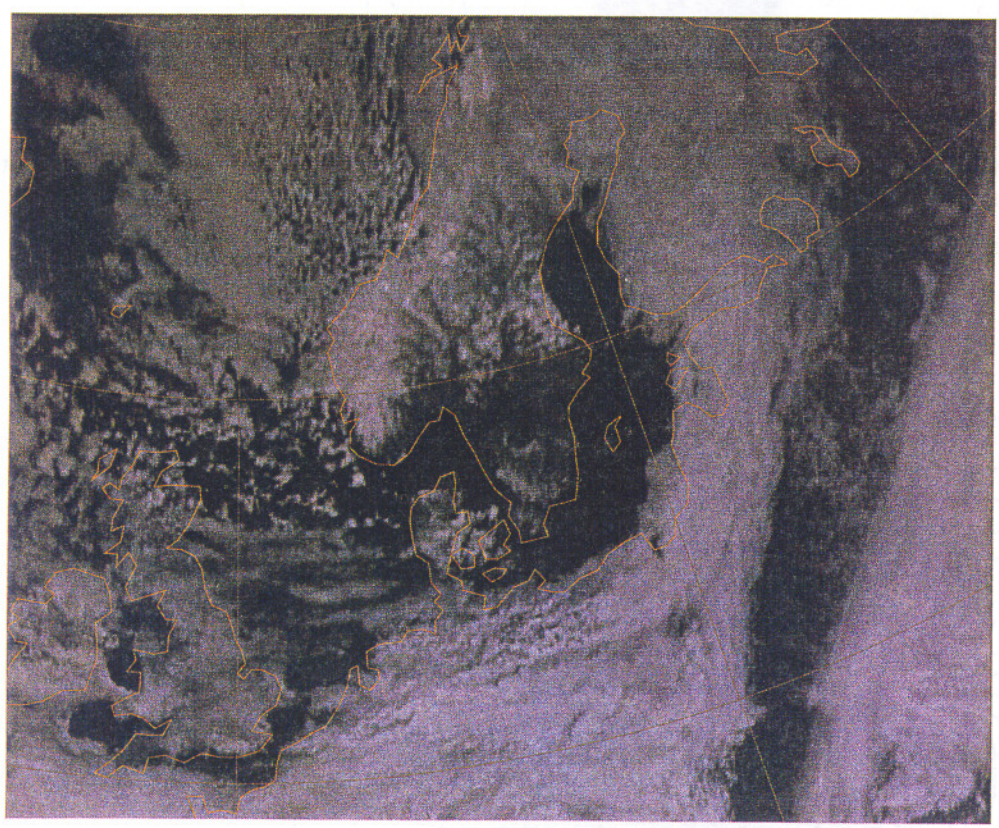

Figure 5: Visible picture for 18 March 1998, 1200 UTC

The surface pressure forecast from the control experiment for this time is shown in Figure 6:

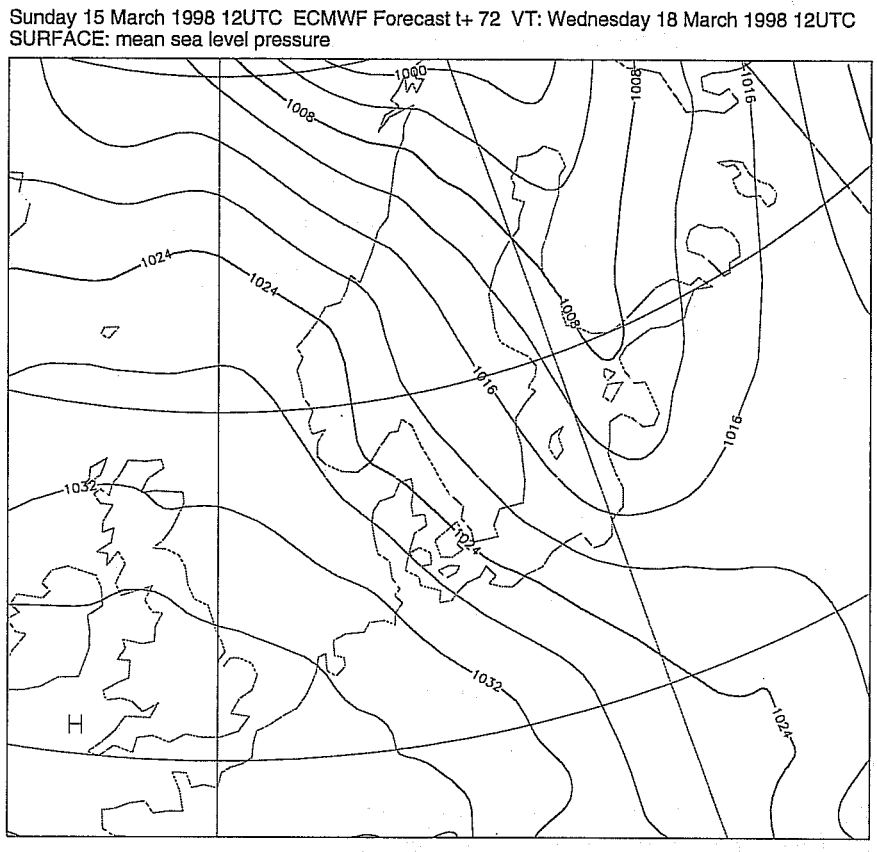

Figure 6:

This shows a broad north-westerly airstream over Norway. Cross-sections of vertical motion from 66N 8W to 59N 18E are shown in Figure 7: for the control experiment and Figure 8: for experiment 4. The results for experiments 2,3 and 5 were very similar to the control.

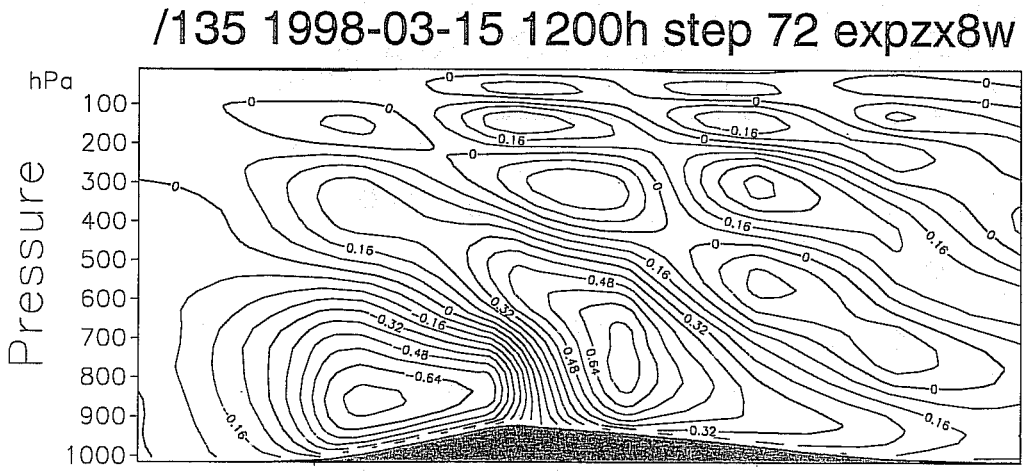

Figure 7: Vertical velocity (Pa s^{-1}) for control experiment

In an additional experiment, the model was run with a 200s timestep rather than the normal 1200s. The cross-section was hardly altered, showing that numerical inaccuracies were unlikely to have generated the wave. Figure 7: shows a mountain wave structure on the scale of the resolved orography. The low level vertical motion on the upstream side represents that required for the low level air, which was flowing at about flowing at 15ms^{-1}, to cross the barrier. On the downstream side there is clearly some form of jump forming. In Figure 8: the wave is eliminated and the structure of the low level flow on the downstream side is altered to remove most of the jump structure. Since there is strong flow through the wave pattern, it is not surprising that a method which smooths along trajectories removes the wave.

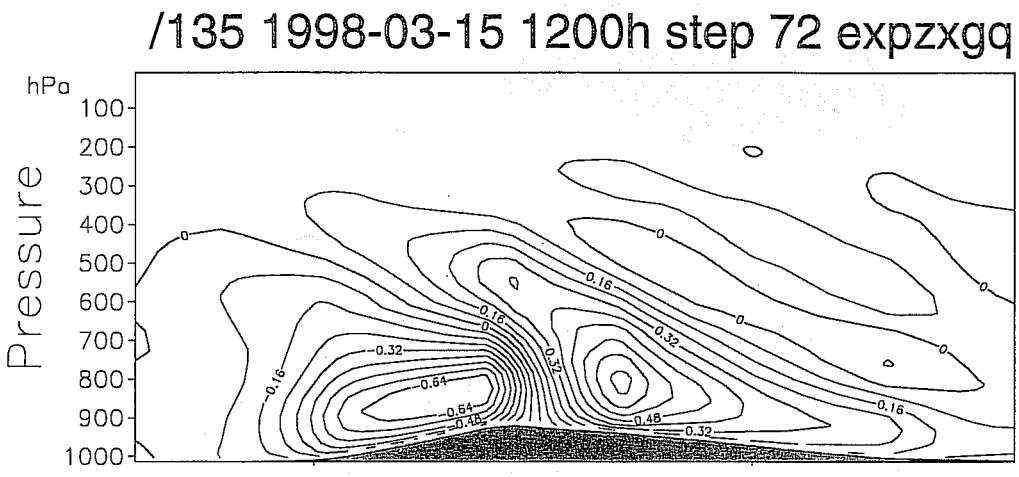

Figure 8: Vertical velocity (Pa s^{-1}) cross-section from experiment 4

The most likely explanation of the result is that the model has produced the correct response to the smooth orography that it has available. The disagreement with the true solution reflects the lack of resolution of the orography. Further work is being carried out with idealised models to investigate this. It remains to be considered whether it is better to smooth out the 'spurious' waves, or whether to retain them because they may contain useful large scale information.

3.6 Behaviour near mid-latitude fronts

This example is a frontal wave crossing Northern France in January 1998. The rainfall accumulated over 24 hours from the control forecast is shown in Figure 9: Shading levels are at 2,4 and 8mm.

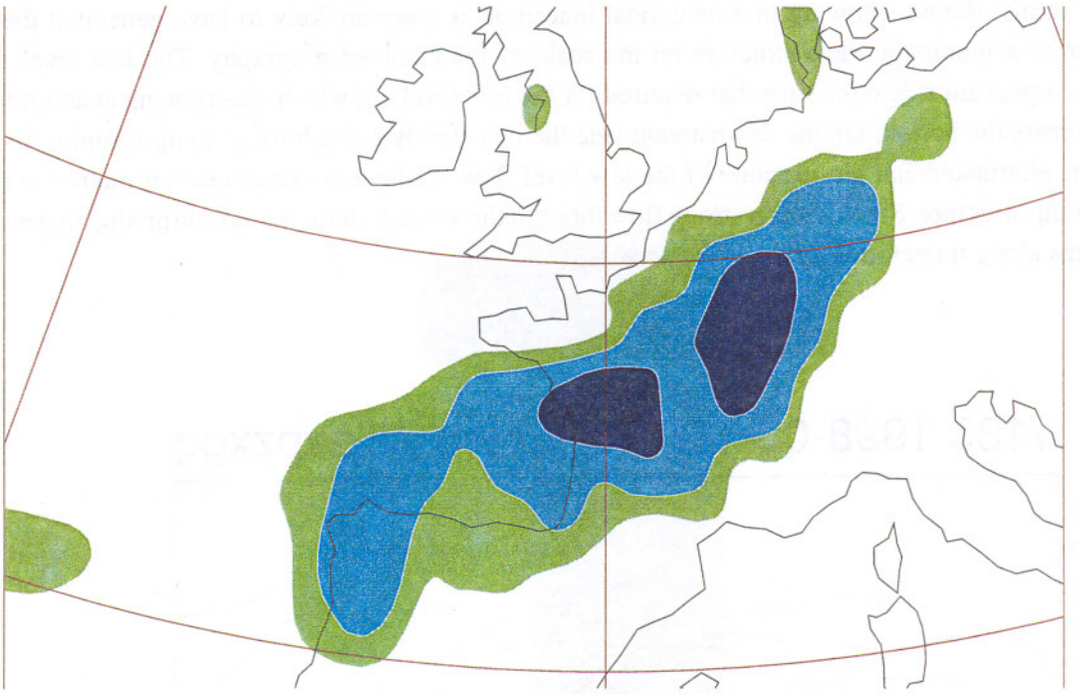

Figure 9: Large scale precipitation accumulation for 24 hrs ending 15 January 1998.

As would be expected from the statistics, all experiments gave similar forecasts. That from experiment 5 is shown in Figure 10:, because this experiment had the largest effect on total rainfall. The area of heaviest rainfall is slightly reduced, and the boundary of the area with rain is slightly smoother.

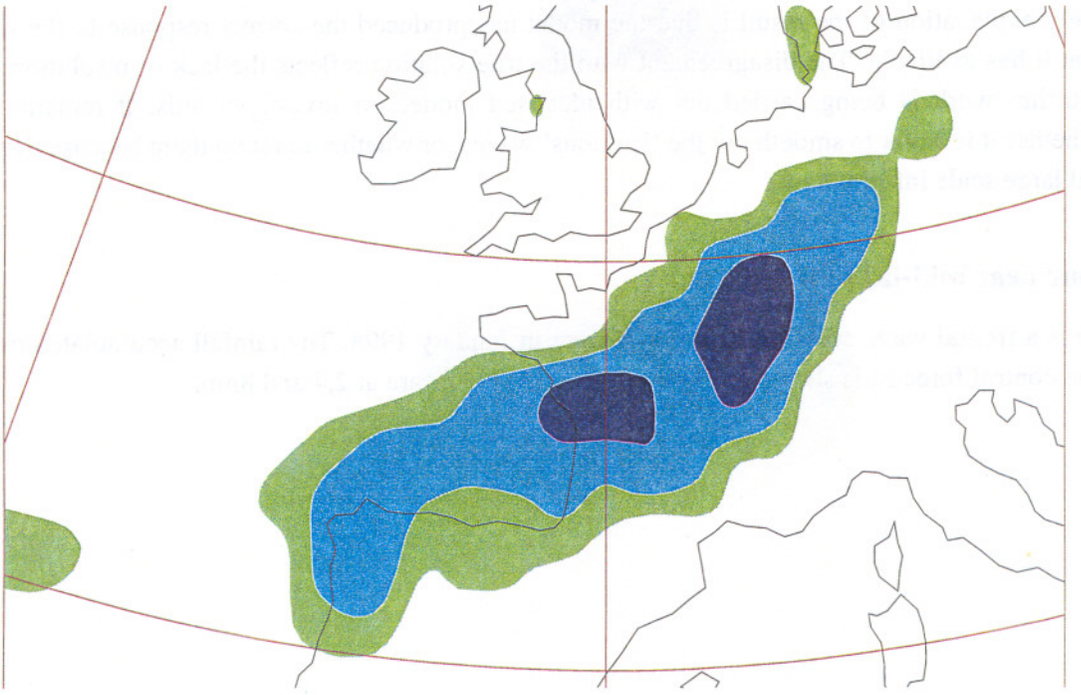

Figure 10: As Figure 9: for experiment 5.

Cross sections of the vertical motion from the two experiments are shown in Figure 11: and Figure 12: The cross section was from 51N 3W to 40N 3E (roughly Cornwall to Marseilles). The maximum value is 12.5% less in Figure 12:, though the qualitative pattern is not changed.

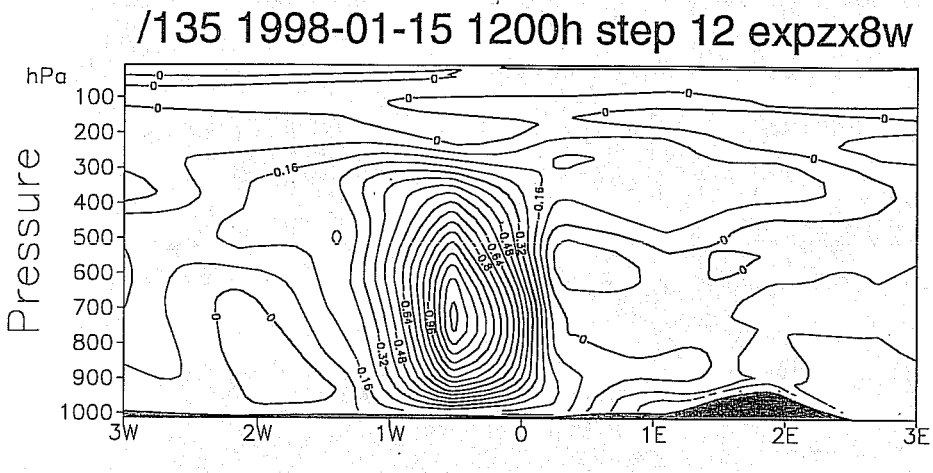

Figure 11: Cross section of vertical motion for control experiment

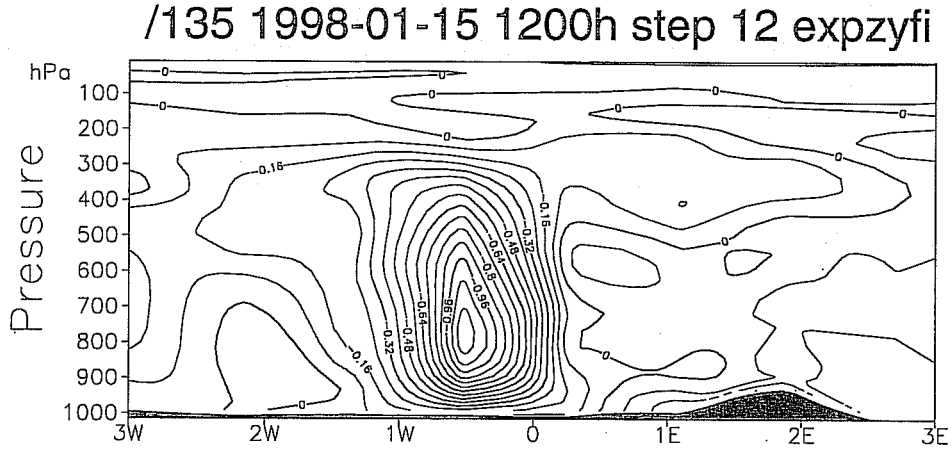

Figure 12: Cross section of vertical motion for experiment 5

This example suggests that the integration techniques tested have little impact on frontal structure and precipitation extent. However, maximum precipitation intensities are sensitive to some extent, and, with higher resolution models able to resolve more extreme precipitation rates, more care may have to be taken with the integration scheme and the interfacing to the physics.

3.7 Behaviour near tropical convection

This example was taken over the tropical ocean to avoid the extra complicating factors over land, such as topography, surface moisture availability, and a stronger diurnal cycle. The satellite picture for 1200 UTC on

18 March 1998 is shown in Figure 13: This shows several bands of convection over the Indian Ocean. The picture taken 6 hours earlier also shows these bands.

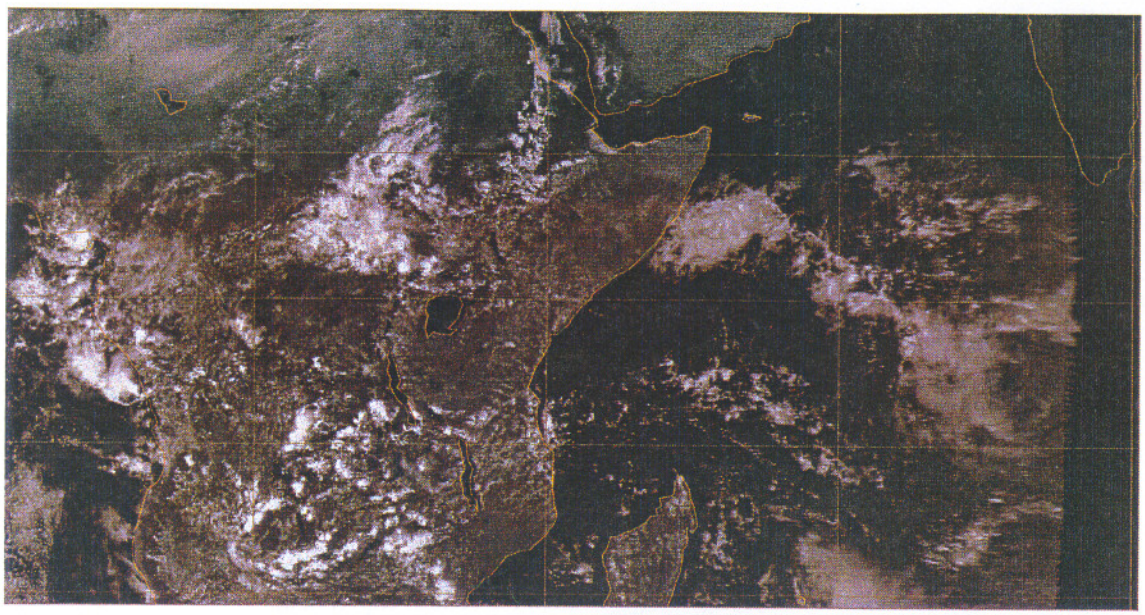

Figure 13: Visible satellite picture for 1200 UTC, 18 March 1998

The 12 hour accumulated convective precipitation from a 72 hour forecast from the control experiment is shown in Figure 14: The banded structure is well predicted, though the individual positioning is not exact. However, precise forecasting of such structures at T+72 is not to be expected, and in any case proper verification over the full 12 hour period is not available.

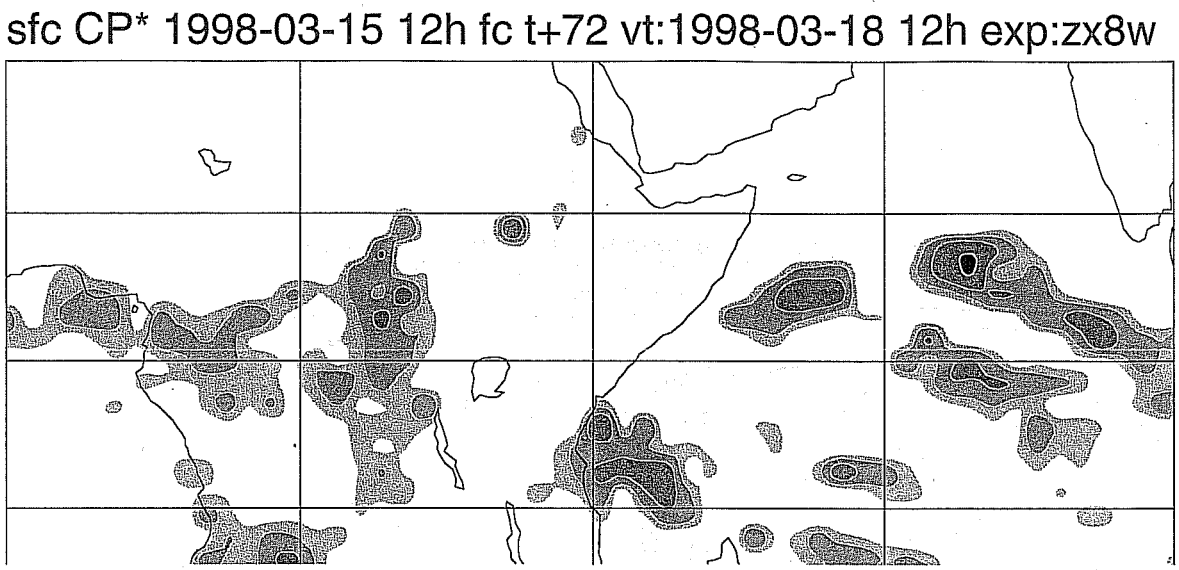

Figure 14: Convective precipitation accumulated from T+60 to T+72, control experiment

All the experiments produced similar structure. Experiment 3 is illustrated, because the global statistics indicated that this experiment gives increased tropical convective precipitation, and increased temporal variability in the tropical vertical motion. The convective precipitation forecast is shown in Figure 15: The increased intensity and area are visible, but the general structure is not affected.

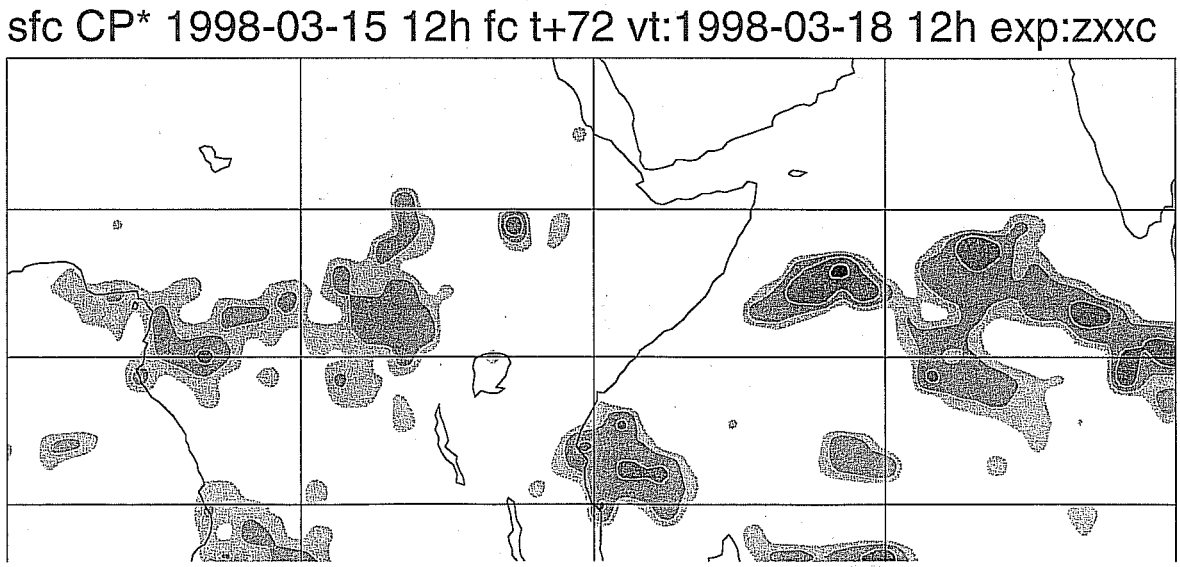

Figure 15: As Figure 14: for experiment 3.

The vertical velocity cross sections along a line from 11N 76E to 19S 57E are shown in Figure 16:and Figure 17: There are localised maxima of upward motion in the convective bands in the upper troposphere, and downward motions near the melting level. It is most likely that these mirror the combined heating and cooling effects of the convection and large scale cloud schemes. To a first approximation, the resolved adiabatic heating must cancel the parametrised heating in the tropics in order to prevent the formation of unsustainable horizontal pressure gradients.

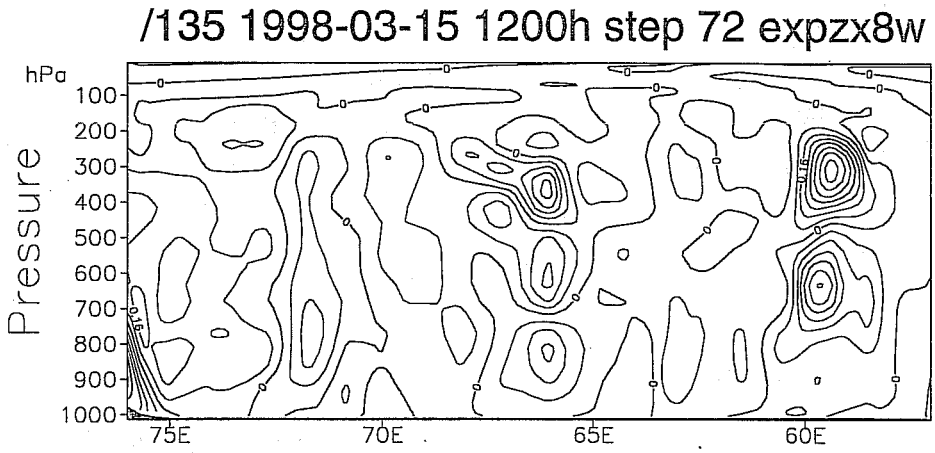

Figure 16: Vertical velocity cross section from control experiment

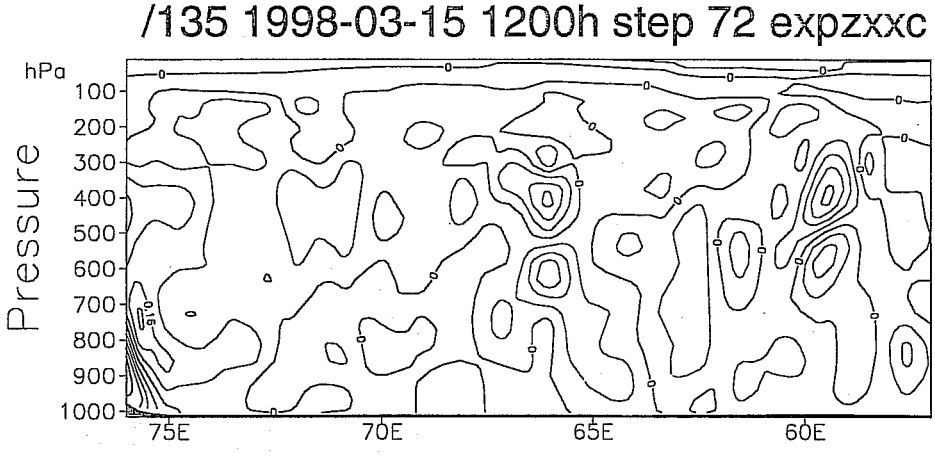

Figure 17: Vertical velocity cross section from experiment 3

4. SUMMARY

This paper has illustrated how diagnostic calculations based on dynamical theory can elucidate the behaviour of the model, and point to areas that need further investigation. Several issues arose repeatedly during the study. There is aliasing of fast wave activity to the model timestep, and possible increased fast wave amplitudes

resulting from the reduction in timescale separation. There are substantial low frequency unbalanced motions on larger space scales than observed, because the motions have to be present to maintain large scale balances, and can only occur on resolved scales. The interfacing of the physics with the dynamics can have a large effect on the high frequency behaviour.

REFERENCES

Browning,G.L. and Kreiss,H.-O., 1986: Scaling and computation of smooth atmsopheric motions. *Tellus*, **38A**, 295-313.

Ford,R., McIntyre,M.E. and Norton,W.A., 1999: Balance and the slow quasi-manifold: some explicit results. *J. Atmos. Sci.*, submitted.

Houtekamer and Mitchell, 1998: Data assimilation using an ensemble Kalman filter technique. *Mon. Weather Rev.*, **126**, 796-811.

Mohebalhojeh,A.R. and D.G.Dritschel, 1999: On the representation of gravity waves in numerical models of the shallow water equations. *Quart. J. Roy. Meteor. Soc.*, submitted.

Parrish, D.F. and Derber,J.C., 1992: The National Meteorological Center's spectral statistical interpolation analysis system. *Mon. Weather Rev.*, **120**, 1747-1763.

Simmons,A.J. and Temperton,C.,1997: Stability of a two-time-level semi-implicit integration scheme for gravity wave motion. *Mon. Weather Rev.*, **125**, 600-615.

Wedi,N.P., 1999: The numerical coupling of the physical parametrizations to the 'dynamical' equations in a forecast model. *ECMWF Tech. Memorandum* no. 274.

Temperton, C., 1997: Treatment of the Coriolis terms in semi-Lagrangian spectral models. In "Numerical Methods in Atmospheric and Oceanic Modelling: The André J. Robert Memorial Volume" (ed. C.A. Lin, R. Laprise and H. Ritchie), 279-292.